Materials Science and Technology (MS&T) 2013
October 27-31, 2013, Montreal, Quebec, Canada

3D MICROSCALE CHARACTERIZATION AND CRYSTAL-PLASTIC FE SIMULATION OF FATIGUE-CRACK NUCLEATION AND PROPAGATION IN AN ALUMINUM ALLOY

A.D. Spear[1], S.F. Li[2], A.R. Cerrone[1], J. Lind[3], R.M. Suter[3], A.R. Ingraffea[1]

[1]Cornell University; 640 Rhodes Hall; Ithaca, NY, 14853, USA
[2]Lawrence Livermore National Laboratory; 7000 East Avenue; Livermore, CA, 94550, USA
[3]Carnegie Mellon University; 6406 Wean Hall; Pittsburgh, PA, 15213, USA

Keywords: fatigue crack, aluminum, X-ray diffraction, tomography, crystal plasticity, finite-element analysis

Abstract

Critical steps toward designing and developing modern materials include observing, simulating, and predicting 3D deformation and cracking mechanisms at various length scales. In this work, advanced characterization and simulation techniques are employed to study the micromechanisms involved in nucleation and propagation of fatigue cracks in an aluminum alloy used in pressure-vessel structures. In addition to electron-backscatter diffraction and scanning-electron microscopy, post-mortem (ex-situ) X-ray tomography and high-energy X-ray diffraction microscopy are used to characterize in 3D the microstructural features, including grain geometries and orientations, local to crack surfaces. Digital reconstructions (viz. 3D crystal-plastic finite-element models) are generated as a way to simulate the observed crack-evolution behavior and thereby compute local response fields along measured crack fronts in 3D. A better understanding of deformation and cracking mechanisms in 3D at the microscale will allow for better predictive modeling, which will be essential to both expedite and expand materials design.

Introduction

Coupling advanced, three-dimensional, experimental and numerical-modeling techniques at the microstructural-length scale provides an understanding of existing-material behavior and enables the design of new materials with optimal properties (e.g. for fatigue resilience). The objective of this paper is to report progress on an ongoing effort to quantitatively relate crack-evolution behavior in an aluminum alloy to local, microstructure-dependent fields by simulating observed, three-dimensional, fatigue-crack evolution. The study of naturally nucleated fatigue cracks in multiple specimens is enabled by using ex-situ characterization

techniques, including fractography, post-mortem X-ray tomography, and post-mortem high-energy X-ray diffraction microscopy (HEDM). The observed fatigue-crack evolution within measured microstructural volumes is then digitally reconstructed using three-dimensional finite-element modeling as a way to compute local, microstructure-dependent fields along three-dimensional crack fronts. A crystal, elasto-viscoplastic material model is implemented within the finite-element framework to predict hetergeneous deformation dependent upon individual grain orientations. Simulating the observed fatigue-crack evolution in the poly-crystalline material remains the subject of ongoing work.

The engineering application of interest in this work is ultrathin aluminum-alloy liners used by NASA to line the inside of ultralight composite-overwrapped pressure vessels [1]. Ultrathin (e.g. $\leq$500 μm thick) liners are of particular interest for several reasons: (1) ultrathin liners are considered state-of-the-art; (2) the microstructural mechanisms governing fatigue-crack nucleation and subsequent through-thickness propagation are not very well understood; and (3) consequences of fatigue-crack evolution within an ultrathin metallic liner could compromise the integrity of the composite overwrap and result in catastrophic failure for both the pressure vessel and possibly the structure containing it.

This work has implications not only for the design of ultrathin pressure-vessel liners, but for the design of new, fatigue-resilient materials. Many of the experimental and numerical methods used in this work can be applied to other important structural materials.

Material and Experimental Method

Material and Specimens

The material used in the study is an Al-Mg-Si alloy received in the form of a cylindrical, nominally thick, pressure-vessel liner. As shown in Fig. 1, significant microstructural variation is observed along the length of the cylinder. Processing details of the liner are provided in [2]. Mechanical properties of the material were determined according to standardized tensile tests [3] using subscale dogbone specimens machined from the central region of the cylinder. The resulting uniaxial, macroscopic, stress-strain curve is provided in Fig. 1.

In the current study, two specimens from opposite ends of the cylindrical region were examined. Specimen S1 was extracted near the port dome (see upper inverse pole figure [IPF] map in Fig.1), and specimen S2 was extracted near the closed dome (see lower IPF map in Fig.1). The specimens were machined from the cylindrical region using wire electric discharge machining (WEDM). The z-ϕ surfaces were then planed by mechanical milling. Finally, WEDM was used to create a single, shallow notch, thereby reducing the minimum thickness in the gauge region to 500 μm. After machining, specimens were chemically milled[1] and subsequently electropolished to a final gauge-region thickness of 400 μm ($\pm 10 \mu m$). Specimen

[1]The chemical milling procedure and its effect on fatigue-crack initiation and total life are detailed in [2].

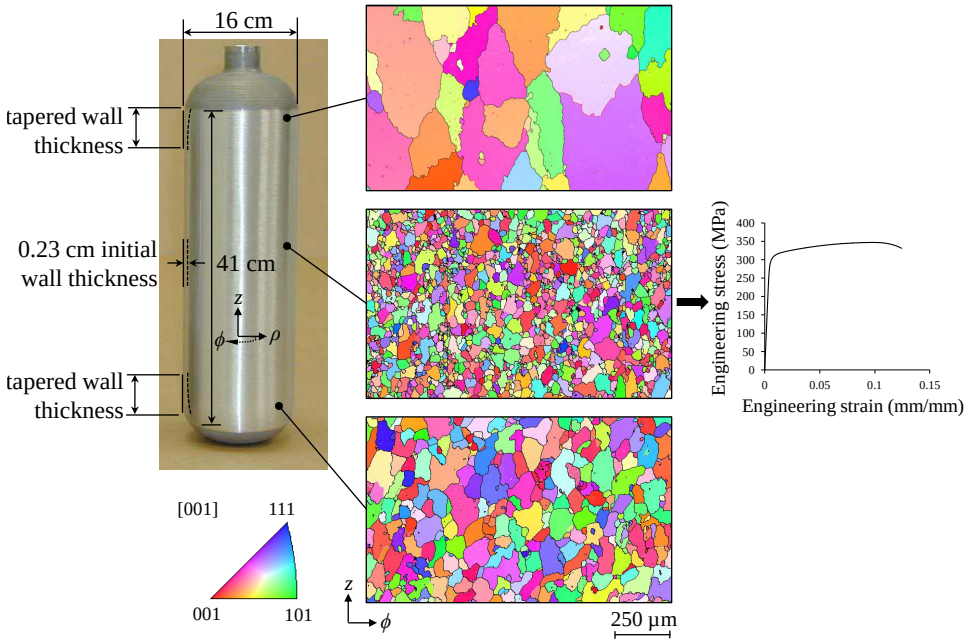

Figure 1: As-received pressure-vessel liner showing approximate dimensions and cylindrical coordinate system (z, longitudinal; ρ, radial; ϕ, tangential). Inverse pole figure (IPF) maps show microstructural variation along cylinder. Stress-strain curve generated from standardized tensile tests [3] using subscale dogbone specimens machined from central region of liner.

dimensions are given in Fig. 2. EBSD measurements were made on the notched surface in a 1 mm-high band spanning the thinnest region, where crack nucleation was expected.

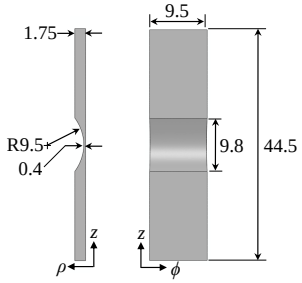

Figure 2: Dimensions (mm) of the single-shallow-notch fatigue specimens.

Fatigue Testing

Each specimen was cycled under load-control using a loading spectrum designed to generate marker bands on the crack surface. Marker banding is a post-mortem technique to retroactively measure subsurface crack-growth rates by mapping the shape of crack-front profiles at programmed cycle intervals [4]. Although marker banding has typically been used for self-similar, long-crack growth, Burns, *et al.* [5], recently used marker banding to characterize crack evolution near crack-initiation sites in an aluminum alloy. Based on the loading spectrum in [5], the following loading sequence was applied to specimens S1 and S2 and repeated

until failure: 10,000 baseline (growth) cycles at $R = 0.5$ + eight-banded marking series + 10,000 baseline cycles at $R = 0.5$ + six-banded marking series + 10,000 baseline cycles at $R = 0.5$ + four-banded marking series, where R is the applied-loading ratio, P_{min}/P_{max}. Each marking series consists of 25-cycle loading blocks that alternate between $R = 0.1$ and $R = 0.5$ to generate the number of aforementioned marker bands. The maximum-applied load, P_{max}, was maintained at 1.0 kN, which results in a maximum-principal notch strain around 1.0% (based on digital-image-correlation data). The applied-loading spectrum generates a unique marker band on the crack surface every 10,000 loading cycles. The marker-banding technique was supplemented by periodically (typically every 50,000 cycles) interrupting the fatigue test, carefully bracing then removing the specimen from the load frame, and imaging the specimen using scanning-electron microscopy (SEM). Doing so provided a surface snapshot of crack length(s) at known cycle counts to correlate with distinct marker bands identified on the crack surface after failure.

Post-mortem Characterization

Fractography and Marker-band Analyses Fractography and marker-band analyses were performed using SEM. A dominant, crack-nucleation site was clearly identified on each specimen by the appearance of river-like features leading to the site. Marker bands were identified in succession using the programmed marking pattern until the first-detectable band was identified nearest the crack-nucleation site. Figure 3 shows an example of the marker-band analysis for specimen S1. The known marker-band locations were digitized and converted to Cartesian coordinates. The points were then carefully fit using spline functions to create continuous crack-front profiles. The complete and continuous crack-front profiles were then used to quantify three-dimensional crack-growth rates over the entire fatigue-crack surface.

Electron Backscatter Diffraction After marker-band analyses, EBSD measurements were again made on the z-ϕ surface adjacent to the dominant fatigue crack. EBSD patterns were indexed with relatively high confidence near (well within 10 μm) the crack surface, suggesting that damage was localized to persistent slip bands prior to cracking. The quality of EBSD patterns collected near the crack surface also provided a positive indication of the feasibility of using HEDM for grain-orientation mapping in volumes adjacent to fatigue-crack surfaces.

X-Ray Tomography and High-Energy X-Ray Diffraction Microscopy WEDM was used to machine out 1-mm-wide strips containing the dominant fatigue crack in each specimen. Material adjacent to each crack surface was then characterized using X-ray absorption tomography and near-field HEDM at the Advanced Photon Source 1-ID beamline at Argonne National Laboratory. Tomography provided a high-resolution boundary reconstruction, and near-field HEDM provided three-dimensional grain geometries and orientations adjacent to the crack surfaces. The data were then merged to exploit the benefits of each technique. Details regarding microstructure reconstruction from HEDM data are provided in [6, 7].

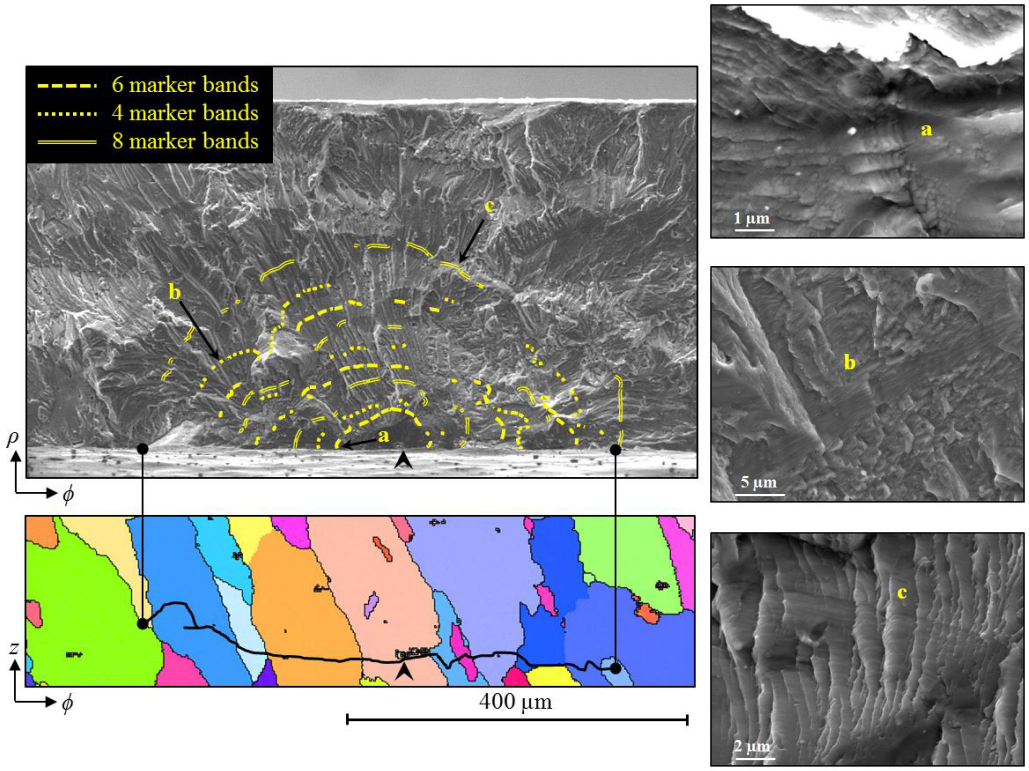

Figure 3: Crack trace imaged at 256,000 cycles shown superimposed on pristine-condition IPF map for S1. Crack tips correspond to outermost marker band shown on ρ-ϕ crack surface above. Black arrowheads indicate location of crack nucleation. Examples of distinct marker bands are shown for locations a, b, and c under high magnification in micrographs at right.

Numerical Modeling

Crystal-plastic Material Model

An elasto-viscoplastic material model is implemented into a finite-element framework according to Matouš and Maniatty [8]. In the model, plastic deformation is manifested by the evolution of slip on twelve octahedral slip systems ({111} <110>) for face-centered cubic materials. Two different hardening-model options are included: precipitation, which gives strong self-hardening, and Voce-Kocks, which gives an equivalent hardness value for all slip systems. For information regarding the model derivation and implementation, see [8].

Material-model Calibration Procedure

Material-model calibration requires texture information and experimental data describing the deformation behavior of a polycrystalline aggregate of the material. Here, monotonic data are assumed to be sufficient since the aggregate, cyclic response of the aluminum alloy after initial loading was found to follow a linear path at R=0.5 (i.e. there was no marked hysteresis response of the polycrystalline aggregate at the applied-load range of interest).

In general, the calibration procedure involves two steps: (1) a high-level calibration of the material-model parameters using a reduced-order material model and (2) a three-dimensional crystal-plastic finite-element (CPFE) simulation to verify the calibrated parameters. An objective function is implemented to perform the first step of calibration. The calibration procedure seeks to minimize the objective function, i.e. the cumulative error between the experimental and simulated stress-strain response of the aggregate. The objective function serves as an interface between a constitutive, material-point simulator written in C++ and the optimization toolbox in MATLAB®. The material-point simulator is an implementation of the elasto-viscoplastic material model described in the previous subsection. The objective function accepts as input a list of grain orientations representative of the material texture and an experimental stress-strain curve. Each material point (i.e. grain orientation in the list) is then passed to the material-point simulator, which returns the response of that point to a given applied-load increment. In this way, the high-level calibration does not account for neighbor effects on each material point. A number of optimization algorithms can be used for the calibration; the current study uses a genetic algorithm to minimize the objective function. Calibrated parameters are then applied to a CPFE model to simulate experimental loading conditions. The software DREAM.3D is used to generate a synthetic polycrystal and surface mesh of the material. The surface mesh is then converted to a volume mesh using a meshing algorithm described in [9]. Figure 4 shows a comparison between stress-strain responses from experiment and simulation for material from the central region of the pressure-vessel liner. The procedure described above can be repeated for the material in specimens S1 and S2 by making adjustments to texture input and macroscopic stress-strain response.

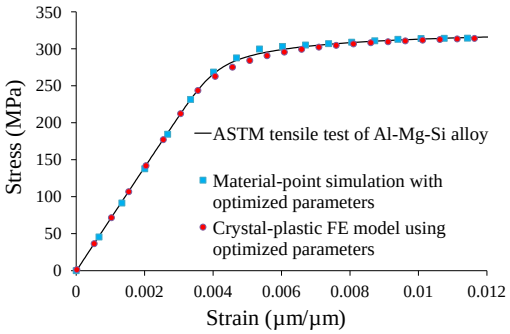

Figure 4: Engineering stress-strain response from standardized tensile tests and simulation.

Results

Despite having identical dimensions, surface treatments, and loading spectrums, S1 and S2 exhibit an 83% difference in total fatigue life, suggesting a strong microstructural dependence. Specimens S1 and S2 failed after 280,000 and 115,000 cycles, respectively. Results are shown for specimen S1 only. X-ray tomography and HEDM reconstructions are shown in Fig.5. Figure 6 shows three-dimensional fatigue-crack-growth rates determined from marker bands (two-dimensional) coupled with X-ray tomography data (three-dimensional). Significant variation in growth rates and directions are observed between and along crack fronts.

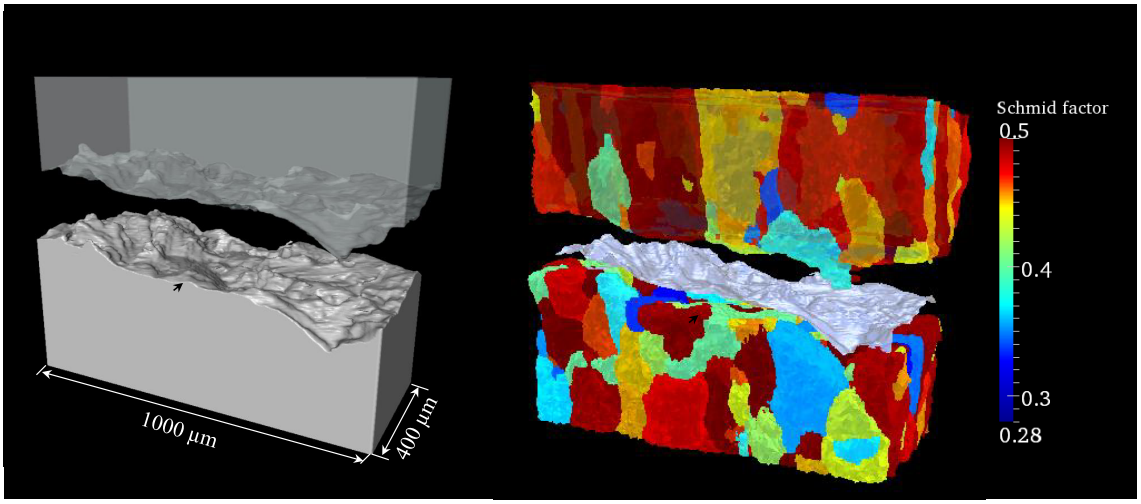

Figure 5: X-ray tomography reconstruction with partial transparency (left) and HEDM reconstruction with overlay of crack surface from tomography (right) for specimen S1. Black arrowhead indicates location of crack nucleation. Grain orientations are described in terms of Schmid factor, where the maximum possible value is 0.5.

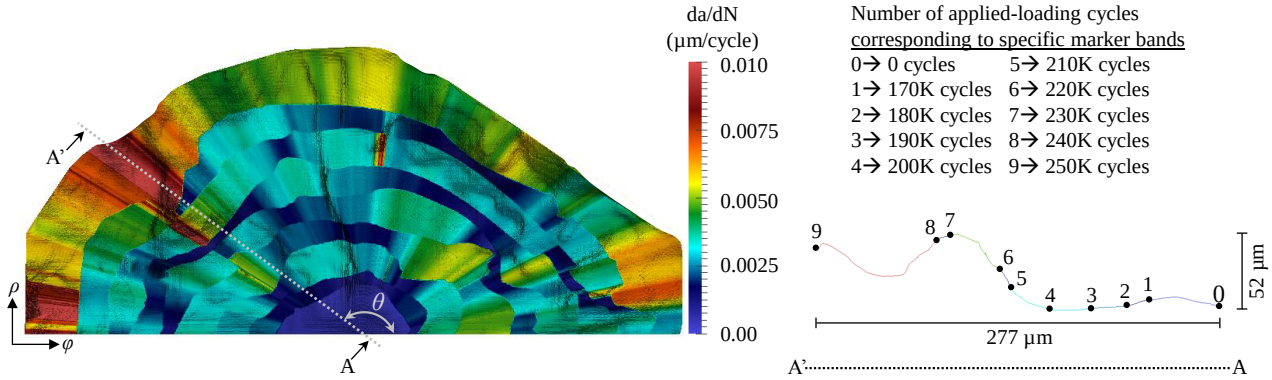

Figure 6: Three-dimensional fatigue-crack growth rates, *da/dN*, for specimen S1. Crack growth is quantified for radial extensions from the crack-nucleation site. For values of θ from 0 to 180°, crack extension, *da*, is calculated as the *total path length* on the crack surface between adjacent marker bands (e.g. between numbered dots shown on section A-A').

Conclusions

Ex-situ techniques were employed to characterize the three-dimensional evolution of naturally nucleated fatigue cracks in an aluminum alloy used in ultrathin liners of composite-overwrapped pressure vessels. Ongoing work involves numerically simulating the observed fatigue-crack evolution in specimens by using three-dimensional CPFE modeling. Simulation results will be post-processed to discover relationships between the underlying microstructures and local crack-evolution behavior. Based on these discoveries, possible recommendations for processing of the ultrathin pressure-vessel liners will be provided.

Acknowledgements

Machining, mechanical testing, and surface characterization were performed at NASA Langley Research Center. This work is supported by the U.S. Department of Energy by Lawrence Livermore National Laboratory under contract DE-AC52-07NA27344; by grant DESC0002001 at Carnegie Mellon University; and by the National Science Foundation under grant No. DGE-0707428 at Cornell University. TeraGrid resources were provided by Texas Advanced Computing Center under grants TG-DMR090022 and TG-MSS110031. Use of the Advanced Photon Source was supported by the U.S. Department of Energy, Office of Science, Office of Basic Energy Sciences, under contract No. DE-AC02-06CH11357. Special thanks to David Littlewood for providing the material-point simulation code. LLNL-PROC-638679

References

[1] P.B. McLaughlan, S.C. Forth, and L.R. Grimes-Ledesma. Composite overwrapped pressure vessels, a primer. *NASA Special Publication NASA/SP-2011-573*, March 2011.

[2] A.D. Spear and A.R. Ingraffea. Effect of chemical milling on low-cycle fatigue behavior of an Al-Mg-Si alloy. *Corrosion Science*, 68:144 – 153, 2013.

[3] ASTM E8-11. Standard Test Methods for Tension Testing of Metallic Materials. American Society for Testing and Materials International, West Conshohocken, PA, 2011.

[4] S.A. Willard. Use of marker bands for determination of fatigue crack growth rates and crack front shapes in pre-corroded coupons. *NASA/CR-97-206291*, December 1997.

[5] J.T. Burns, J.M. Larsen, and R.P. Gangloff. Effect of initiation feature on microstructure-scale fatigue crack propagation in Al-Zn-Mg-Cu. *International Journal of Fatigue*, 42:104 – 121, 2012.

[6] R.M. Suter, D. Hennessy, C. Xiao, and U. Lienert. Forward modeling method for microstructure reconstruction using X-ray diffraction microscopy: Single-crystal verification. *Review of scientific instruments*, 77(12):123905–123905, 2006.

[7] S.F. Li and R.M. Suter. Adaptive reconstruction method for three-dimensional orientation imaging. *Journal of Applied Crystallography*, 46(2):512–524, 2013.

[8] K. Matouš and A.M. Maniatty. Finite element formulation for modelling large deformations in elasto-viscoplastic polycrystals. *International Journal for Numerical Methods in Engineering*, 60(14):2313–2333, 2004.

[9] J.B. Cavalcante Neto, P.A. Wawrzynek, M.T.M. Carvalho, L.F. Martha, and A.R. Ingraffea. An algorithm for three-dimensional mesh generation for arbitrary regions with cracks. *Engineering with Computers*, 17(1):75–91, 2001.